



IJITCE

ISSN 2347- 3657

International Journal of Information Technology & Computer Engineering

www.ijitce.com



Email : ijitce.editor@gmail.com or editor@ijitce.com

1,1-BI-2-NAPHTHOL SOLUTIONS UNDER UV-NEAR-RESONANCE RAMAN SCANNING

Ms.Wazida Begum

Association professor

Department Of H&S

NAWAB SHAH ALAM KHAN COLLEGE OF ENGINNERING & TECHNOLOGY

NEW MALAKPET , HYDERABAD-500 024

ABSTRACTS

Measurements of the normal and UV near-resonance Raman spectra of BN in basic solution were made and analysed, and the results were published. Ground state geometry, vibrational frequencies, off-resonance Raman intensities and depolarization ratios of 1,1-bi-2-naphtholate dianion were studied using density functional theory (DFT) computations (BN2-). The observed Raman bands were allocated in detail based on the estimated and experimental findings of \hat{i} , I , and F . UV resonance Raman spectra showed a substantial increase in the 1612 cm^{-1} Raman band of BN compared to the conventional Raman spectrum. According to depolarization ratios for the 1366 and 1612 cm^{-1} bands, it is clear that both transitions polarizabilities contribute to the 1366 cm^{-1} band, whereas only transitions polarizabilities contribute to 1612.

Introduction[=

Chemists and biochemists depend heavily on chiral compounds. Because of their very stable chiral conformation, chiral 1,1-binaphthyl compounds have become more popular. Asymmetric organic synthesis and catalytic processes have previously used them extensively as chiral inducers. 1,2 1,1-bi-2-naphthol (BN) and its derivatives, which are optically active, are particularly important C₂-symmetric molecules. 1,1-bi-2-naphthol is widely used as a starting point for the production of chiral binaphthyl compounds, on the other hand. It has been frequently employed as ligands for asymmetric metal complexes and has proven excellent performance in chiral recognition with this particular type of chemical. 3-6 Using chiral binaphthol-derived titanium complexes, Ishii et al. studied asymmetric catalysis of the Friedel-Crafts process with fluoral. 5a The steric and electronic characteristics of the chiral BN ligands influence the result of a specific asymmetric transformation. It has been extensively researched using several spectroscopic approaches, including as electronic absorption, IR, and Raman spectroscopies, to determine its structure and characteristics. The VCD spectra of BN were measured by Setnicka and coworkers, who then used density functional theory (DFT) computations to assign the observed VCD bands. 7 Calculations based on DFT were used to investigate the mechanism of BN isomerization. 8 BN adsorbed on silver colloids was examined by Nogueira and coworkers for the first time using surface-enhanced Raman (SER) spectroscopy, and empirical assignments for the observed Raman bands were provided. 9 Due of its near-UV absorption, the UVRR spectrum of BN in diverse solutions is likely to be observed and may give information on both the ground and excited states. But to our knowledge, the resonance Raman (RR) spectra of BN have not yet been reported in the literature. While this is the case, new spectroscopic methods for probing molecule chirality, sum-frequency generation (SFG) of chiral solution, are now under development as novel spectroscopic tools¹⁰⁻¹⁸. These tools were reviewed by Belkin and Shen^{17a} and Fischer and Hache^{17b}. The chiral sum-frequency spectroscopy of electron transitions,^{12,15} the chiral sum-frequency spectroscopy of vibrational transitions, and the doubly resonant SFG (DR-SFG) have all been used to investigate R(S)-BN solutions as a prototype for chiral compounds. The new chiral electrooptic effect: SFG from optical active BN liquids in the presence of a dc electric field,¹⁶ as well as second-harm Many aspects of the sum-frequency vibrational spectroscopy (SFVS) studies of chiral BN solution are shared by resonance Raman spectra of BN solution. To begin, the Placzek invariants 1 for vibrational peaks in RR spectra show that the intensity of the chiral vibrational peaks in infrared-visible sum-frequency vibrational spectra from isotropic chiral liquids is proportional to the square of the corresponding antisymmetric Raman tensor element¹⁴. 20 Using direct resonance Raman spectroscopy, it is possible to investigate the relationship between the SFG and the antisymmetric Raman

tensors. As a second example, substantial resonance enhancement, thorough mode assignment, and the ability to deduce vibronic coupling for the modes are all benefits of using RR spectroscopy for sumfrequencies in the vibrational spectrum. 14,15.1,1-bi-2-naphthol has been studied in a basic solution for its UV near-resonance Raman spectra. Intensity and depolarization ratio resonance enhancements, and the 1612 cm⁻¹ and 1366 cm⁻¹ antisymmetric Raman tensors. Vibrational bands in RR spectra have been analysed qualitatively. Researchers have used DFT simulations to investigate the 1,1-bi-2- ground state structures and vibrational spectra. Naphthol and 1,1-bis-2, naphtholate dianion, respectively (BN²⁻), because the two hydroxyl groups of BN may interact with one other in a basic solution take place, leading to the formation of BN²⁻. 1,6 assigning a number of molecular vibrational bands. BN spectra are shown here. in a succinct and reasonable manner particular tasks rather than a review of the literature. 7,9,18. A search for vibrational spectra of Bn and Bn₂ did not provide any results, 9,14. Assignments of Raman bands for BN are discussed in this study. BN₂ and BN₃ have been addressed in further depth. Combining polarisation and DFT calculations results from experiments and BN₂-Raman spectra compared with the one of BN.

Experimental and Computational Methods

Without additional purification, 1,1-Bi-2-naphthol was acquired from Alfa Aesar and utilised in the experiment. Dissolving BN in 3 M NaOH aqueous yielded the BN²⁻ and BN solutions. the concentration of acetone solvents, respectively, from 0.3 to 0.05 molars. The solutions that had been devised were permitted to 3 days of equilibration before spectral measurements are recommended. Light paths of 5 mm were used to collect UV-vis absorption spectra, utilising a Shimadzu UV-C cell at ambient temperature. The spectrometer 2401PC is used for this analysis. A Jobin-type instrument was used to capture the Raman spectra. Probe fitted with air-cooled cooling system: Labram HR 800 spectrometer Scanner with 600 grooves/mm and a CCD detector a 2400 grooves/mm UV grating and a visible grating. AA 40 mm lens was utilised to capture the occurrence in its entirety. back-scattering of a laser beam to gather the scattered light geometry. The 325 nm and 514.5 nm lines of a He-Cd laser. An Ar ion laser's nm line was employed as the excitation source for this experiment. The sample was powered at 3.5 mW and 1 mW. The CCD detector's data collecting duration ranged from 80 to 180 s. Spectra of the Raman effect. To limit the chance of the sample being harmed as a result of exposure. We found UV levels after continuous exposure to laser light. resonance. A revolving cell is used to get the Raman spectra of a solution. Raman band depolarization ratios were analysed using the identical circumstances apply. The components that are perpendicular and parallel

samples of solution polarised Raman spectra parallel and perpendicular, polarizers were used in accordance with the laser's incident polarisation beam. Because the spectrometer does not have polarisation capabilities, the polarised scrambler avoids biases in polarisation detection. Both tetrachloromethane and cyclohexanes were studied for their Raman scattering properties. the depolarization ratios of the were checked and calibrated by measuring. Species of interest. DFT computations were performed on BN and BN²⁻ molecules. out of the three-parameter hybrid functional developed by Becke et al. (known as B3LYP),²¹ has been used for research purposes. BN systems' structures and characteristics.^{8,18} To cut back. We began our search for stable states with a low computational cost in mind. geometric optimization of the examined molecule's structure using Basis sets of 6-31G, which do not have any symmetry, constraint. The final structures created from the collected data were then Using 6-31G* basis sets with the appropriate symmetry to optimise. A limitation on the (C₂ point group). Calculations based on the analysis of frequency (with B3LYP/6-31G*) the final touches on the optimal structure had been completed in order to verify that the optimised structures are really energy-efficient. a theoretical vibrational spectrum may be obtained by combining these two methods. As a result of indifference to anharmonicity and incomplete base sets. Vibrational frequencies are often underestimated when using DFT calculations. frequencies. Differences between the calculated and actual values. This may be scaled to adjust for both experimental and natural frequencies.

A single factor was used to compute the frequencies. a study by 23 Oakes et al. it has been recommended that the standard value of 0.98 be used. The porphyrins are an example of planar conjugate systems.²³ This element has a significant impact on the outcome. is used in this research. Assigning each person's vibrational frequency. Checking the Cartesian frequency was used for this purpose. movements in the regular mode of the relevant object. All of the

computations have been done. Gaussian 03 suite 26 was used for the experiments. using a P4-3.0G processor We use isolated single molecule calculations in this study. to anticipate the shape and frequency of solution-phase vibrations. If there are any mistakes or discrepancies, it may not be accurate. For a dianion, this is very important. However, at this point in time, the situation is rather different. literature on quantum mechanics tends to emphasise practise over theory. computations in chemistry. As an example, using a similar method Accomplished ab initio computing was created by Markham et al. treatment of the resonance effect of deuterium replacement Imidazole, imidazolium, and their derivatives' Raman spectra, When the solvent impact is high, it's likely to be at least 22 in contrast to what was found in this research. theoretical computations by Pasterny et al. showed that the computed results had not changed significantly The relationship between vibrational frequencies and medium polarity.

Results and Discussion Ground-State Geometries and Atomic Charges.

The ground-state geometric structure of BN₂ was studied using DFT calculations. Calculations show that BN₂⁻ is the best candidate. Figure 1b shows that it possesses a trans-quinonoid-like structure. This is in line with the fundamental BN experiment's findings. solution. 1.6 Table 1 shows the bond lengths, bond angles, and bond numbers. B3LYP/6-31G* was used to improve the dihedral angles of BN₂. For In order to provide a point of reference, the BN structure was also estimated. outcomes were reported at the same theoretical level Results from X-ray crystallography are shown in Table 1. Graph No. 27 The BN structure drawing and atomic labelling utilised in Example 1a is shown in Figure 1a. this document Table 1 shows the calculated bond lengths. According to the experimental results, the angles of BN are typically in accord Calculations using the B3LYP/6-31G* formula reveal that The BN molecule's two naphthol rings are almost parallel. They are in agreement with each other. There's a dihedral angle in the plane of 92.7° is compatible with the naphthyl groups' planes. BN. 27 Deprotonation's X-ray value (99.2°) is in line with this. leads to the formation of two naphthyl groups by hydroxyl radicals bent in the direction of coplanarity, leading to rise A more pronounced dihedral angle (68.3°). Calculation of the DFT for BN₂ via alterations in the C-O and C-C bonds are clearly visible. near the hydroxyl groups. When compared to BN, the C1-the distances between BN₂-C2, C2-C3, as well as C9-C10, are determined. while increasing by 0.067, 0.049, and 0.017 The distance between C1 and C9 has been shown to decrease by 0.013 nm. Particularly, BN₂⁻'s C-O bond length drops by 0.105 nm comparing to BN's results based on the bond's calculations BN₂⁻'s dihedral angles and lengths suggest that it has a quinonoid like structure. Figure 1b illustrates the structure. This kind of analysis is called a natural population analysis (NPA). B3LYP/6-31G(d) for BN and BN₂⁻ ground states. Table oxygen and carbon atoms are shown in figure 2 with their respective atomic charge distribution. Both BN and BN₂⁻ have ring carbon atoms. As you can see, C2 is the only carbon atom that does not have a negative charge. This one has a definite electric charge. Calculations based on the NPA show that UVRR Spectroscopic Study of 1,1'-Bi-2-naphthol Solutions

TABLE 1: Calculated Structural Parameters of BN and BN²⁻ and Experimental Values of BN

	BN ²⁻ (calcd) ^a	BN (calcd) ^a	BN (exp) ^b
bond distances (Å)			
C ₁ -C ₂	1.454	1.387	1.382
C ₂ -C ₃	1.467	1.418	1.410
C ₃ -C ₄	1.367	1.373	1.351
C ₄ -C ₁₀	1.423	1.418	1.418
C ₅ -C ₁₀	1.414	1.420	1.426
C ₅ -C ₆	1.383	1.376	1.353
C ₆ -C ₇	1.420	1.416	1.393
C ₇ -C ₈	1.377	1.377	1.369
C ₈ -C ₉	1.437	1.423	1.411
C ₉ -C ₁₀	1.452	1.435	1.423
C ₉ -C ₁	1.417	1.430	1.424
C ₂ -O ₁₁	1.263	1.368	1.370
C ₁ -C _{1'}	1.498	1.495	1.494
bond angles (deg)			
C ₁ -C ₂ -C ₃	115.4	121.3	121.1
C ₂ -C ₃ -C ₄	124.0	120.4	120.2
C ₃ -C ₄ -C ₁₀	120.8	120.8	121.6
C ₁₀ -C ₅ -C ₆	122.1	121.0	121.0
C ₅ -C ₆ -C ₇	118.3	119.7	120.5
C ₆ -C ₇ -C ₈	121.2	120.8	120.3
C ₇ -C ₈ -C ₉	122.5	121.1	121.6
C ₈ -C ₉ -C ₁	122.6	122.1	122.4
C ₁ -C ₉ -C ₁₀	121.8	119.9	119.7
C ₂ -C ₁ -C ₉	120.2	118.8	119.1

TABLE 2: Calculated NPA Charges for BN and BN²⁻

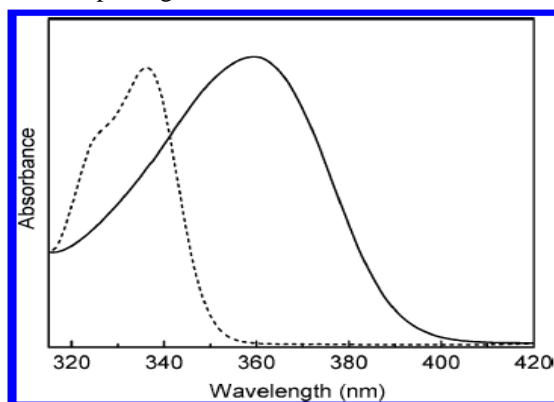
	BN	BN ²⁻
C1	-0.089	-0.145
C2	0.350	0.406
C3	-0.298	-0.298
C4	-0.190	-0.250
C5	-0.204	-0.229
C6	-0.245	-0.323
C7	-0.228	-0.274
C8	-0.214	-0.211
C9	-0.023	-0.028
C10	-0.074	-0.107
O11	-0.680	-0.731

	dihedral angles (deg)		
C ₂ -C ₁ -C ₁ -C ₂	111.1	86.5	
C ₂ -C ₁ -C ₁ -C _y	68.3	92.7	99.2

^aDFT calculations using 6-31G* basis-sets. ^bX-ray results from ref 27.

UV-Visible Absorption Spectra.

Absorption spectra of 1,1-bi-2-naphthol dissolved in acetone and 3 M NaOH aqueous solution are shown in Figure 2 (left) and Figure (right). In the absorption spectra of acetone show two peaks. 324 nm and 336 nm are the best. BN is the primary solution for BN. It moves to 358 nm with an uneven absorption peak. A widened silhouette. It should be noted that the excitonic splitting for BN and BN²⁻ is different because the anion's dihedral angle is no longer around

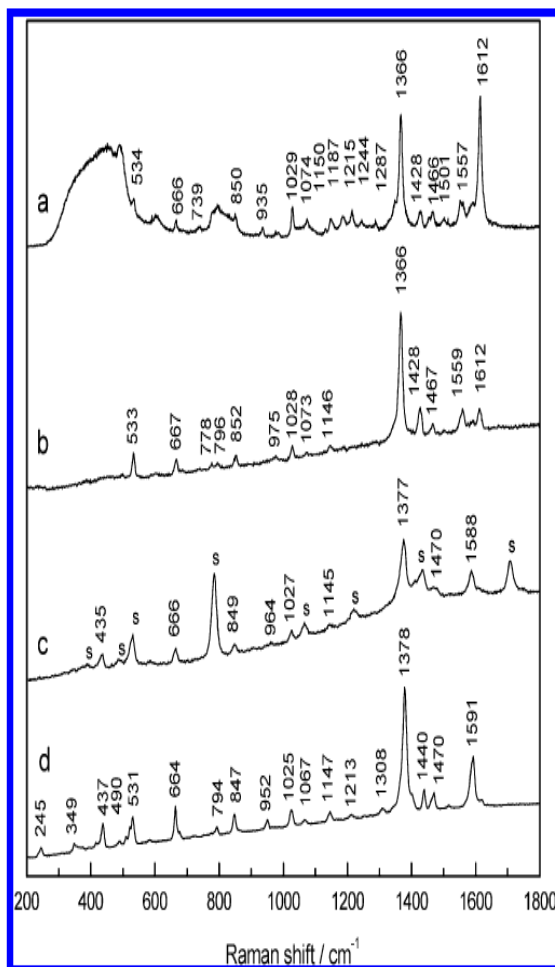


90 degrees, and **Figure 2.** UV-visible absorption spectra of BN in a 3 M NaOH aqueous solution (solid line) and in an acetone solution (dot line).

Larger splits may be induced by this method. There are a number of possible explanations for the wider peak width shown in BN²⁻. The Franck-Condon trend is also a significant contributor to peak width in the spectrum of absorption. The most compelling proof that the doublet's Franck-Condon progression was the electronic spectrum, as recently by Fischer et al.¹⁵, 2HN and BN are certainly chemically similar. It owns up to its own doublet. The solvent impact is also a factor. It is also critical in creating a more rounded silhouette. The colour change from red to basic solution BN's UV absorbance is higher than that of its solution in water. This may be ascribed to the improved electrical properties of acetone on the excited states of BN²⁻, which had been well-known conjugate anionic bases of hydroxyaryls.

Raman Spectra.

BN²⁻ dianion contains 34 atoms and 96 modes of vibration, which, according to the C₂ symmetry, can be categorized as $49A + 47B$. The vibrations of BN molecule, which having two extra hydrogen atoms, may be classed as $52A + 50B$. According to the vibrational selection criteria, all of these modes are active for both IR and Raman transitions. For regular nonresonance Raman, depolarization ratios generally have a value between 0 and 0.75. The depolarization ratio is less than 0.75 for a completely symmetric mode, while it equals 0.75 for a non-totally symmetric mode. As such, polarized Raman measures may be used to estimate the symmetry of a particular mode. Nogueira et al. examined the SERS of BN with 1064 nm excitation and recommended preliminary designations for numerous strong Raman bands.⁹ In this article, the UV resonance Raman spectra and normal Raman spectra of BN in the basic solution were recorded. More full assignments and some reassignment of Raman bands have been created on the basis of DFT computations, polarization measurements, and comparison of Raman spectra of BN²⁻ with those of BN. Figure 3 depicts the typical Raman spectra of BN in an acetone solution or as solid powder with 514.5 nm excitation, normal (exc) 514.5 nm and near-resonance (exc) 325 nm Raman scattering of BN in aqueous NaOH solution, where the Raman emissions owing to the solvent (acetone) are designated as "S". Tables 3 and 4 list the experimentally observed and DFT-calculated frequencies, intensities, depolarization ratios, and assignments of Raman bands of BN and BN²⁻. The tasks will be addressed in depth in the following section 3.3.1. Because of the steric hindrance utilizing OH group and hydrogen bonding in BN solutions,⁷ we treat BN and BN²⁻ as hard molecules and do not construct the average for the dihedral angle between two aromatic planes for dependent qualities. Although a similar method was utilized in certain similar references,^{7,18} additional extensive research are required. A recent work relevant to this has been undertaken by Devlin et al., who thoroughly explored



configurational and

conformational analysis of some chiral molecules using IR and VCD spectroscopies and ab initio density functional theory.

Figure 3. Raman spectrum of BN (a) in a

Raman Spectra Excited at 514.5 nm.

Raman spectra of the BN in 3 M NaOH aqueous solution as well as in acetone stimulated at 514.5 nm are shown in Figure 4. Fig. 5 illustrates. Raman spectra's Cartesian displacements from Based on B3LYP/6-31G*, we've arrived at BN2. Raman spectroscopy reveals BN2- (Figure 4b), a significant Raman band was seen 533, 667, 852, 975, 1028, 1366, 1428, 1467, 1559, and 1592 A density of 1612 cm⁻¹. These bands are seen as a good match for vibrations that are completely symmetrical due to the depolarization ratios that they exhibit less than 0.75. The BN2-band's strongest band could be seen. It seems that the 1377 cm⁻¹ matches to the 1366 cm⁻¹ as seen in Figure 4a) because of the presence of their similar levels of depolarization and intensity. 1064 nm is the wavelength in question. This band was also noticed with an exuberant BN SERS. the C-O stretching was assigned with high severity mode. 9 Our DFT calculation, on the other hand, fails to uncover a sufficient in the area, a possible candidate for C-O stretching contrary to When using the B3LYP/6-31G* formula, an extremely powerful Due to the C9C10/C9C1 stretching mode, Raman is seen at 1357 cm⁻¹. to the naphthalene's structural mode, as per Scherer³⁰). As a result, we assign the 1366 cm⁻¹ band to Vibrational BN2- to the A-symmetry C9C10/A9C1 stretching vibration. A similar way of operation was observed for the neutral BN molecular molecule. A notable Raman intensity was found at 1387 cm-

1. This is quite close to the actual figure that was measured (1377 cm⁻¹). The B3LYP /However, BN's 6-31G* computation shows that this mode is present. Because of the C9C10/C9C1 stretches, the O11-H18 bonds This mode also involves in-plane bending. Because of this, predicted that the -OH group deprotonation would lead to an obvious impact on the frequency of the signal. Predicted results of DFT calculations Deprotonation causes a 30 cm⁻¹ shift in this phase. Experiments revealed an 11 cm⁻¹ decrease in the BN2 has a 1366 cm⁻¹ band, compared to BN, which has a 990 cm⁻¹ band. but still substantially different from the calculated value The theoretical forecast was correct. Three polarised Raman bands may be seen between 1550 and 1650 cm⁻¹. detected at a wavelength of 1559, 1592, and 1612 cm⁻¹ the dianion BN2. Bands 1559 and 1612 cm⁻¹ of BN2- may be seen as A lot more powerful than the 1592 cm⁻¹ range. According to Nogueira et al., The C-C stretching of these bands has been scientifically linked to them. Rings of naphthyl According to our density functional theory (DFT) calculations for the BN2-dianion, notwithstanding the fact that the weak 1592 cm⁻¹ band might be blamed on ring stretching of the naphthyl's C7, 8, 3, 4, and C10, 5 bonds Both the C2O11 and the powerful 1559 and 1612 cm⁻¹ bands are involved. both stretching and the C3C4/C5C6 stretching of naphthyl are used The BN's solid, with a strong 1591 cm⁻¹ band and a weak 1619 cm⁻¹ band. In this area, cm⁻¹ were detected. We believe they're the result of The B3LYP/6- model predicts vibrations of 1606 and 1630 cm⁻¹. Calculation results from the 31G* show that these two modes are linked. mostly by the stretching and bending of naphthyl CC and O11H18, as well as an important contribution from the 1630 cm⁻¹ mode from the stretching of C2O11. Because they both rely on vibrations, The deprotonation of -OH groups is a process that substantial frequency shifts are likely to occur in these two cases. modes. This seems to be the explanation for the apparent disparity between the The 1550-1650 cm⁻¹ range in the BN and BN2-Raman spectra. Most BN and BN2-related vibrations occur between 900 and 1500 Hz. Naphthyl in-plane CC stretching and CC stretching CH is buckling under the strain. At 1467 nm, we found two distinct Raman bands. as well as 1428 cm⁻¹ for BN2 (Figure 3b). In this case, the matching bands For the BN solid, 1470 and 1440 cm⁻¹ were observed A band at 1440 cm⁻¹ is overlapping with BN in acetone solution. It's a solvent band Our DFT calculations reveal the following the CC stretching of naphthyl has been divided into two bands. in-plane bending connected to the C-H through the $\hat{1}29$ Naphthalene may exist in four different forms, according to Scherer's notation³⁰. Downshifts of 1 cm⁻¹ and 35 cm⁻¹ are predicted by DFT calculations. BN2's two modes of operation, as opposed to BN1 The BN. In our experiments, we saw a 3 cm⁻¹ decrease in with a downshift of 12 cm⁻¹ for the 1428 cm⁻¹ With comparison to their BN2 cousins, the band of BN2 is qualitatively identical to what was predicted. At 1146 and 1028 nanometers, we see the Raman bands of BN2- with an in-plane vibration frequency of 975 cm⁻¹ for the naphthyl groups It'll look something like this: at the plane of Scherer's $\hat{1}6$, bending of the C6/C7H stretch of the C6C7 bond, and in-plane deformation, both at $\hat{1}24$ and $\hat{1}32$ of the naphthyl ring kind). According to the B3LYP/6-31G* calculations, for each of these modes was 1143 cm⁻¹, 1024 cm⁻¹, and 975 cm⁻¹. A similar pattern was seen for BN molecules. It was determined that the wavelengths were at 1145, 1027 cm⁻¹, and 964 cm⁻¹. similarity between the frequencies and intensities of and 957 cm⁻¹ BN and BN2-bands show that deprotonation has occurred The CH and CC are only slightly affected by -OH groups. A moderate effect is produced by a short distal benzoring limb stretch. The naphthyl ring's in-plane deformation. As shown by our DFT results, the vibration of BN and This area of 700-850 cm⁻¹ is mostly attributable to the inplane. Naphthyl ring deformations. We add meaning to what we see. Bands 852 cm⁻¹ and 849 cm⁻¹ of BN2 to the 852 cm⁻¹ of BN changes in the shape of the distal benzo ring is mostly attributable to the C3C4C10 expanding out of phase and In other words, the bond angles of C6C7C8. Calculations based on DFT suggest that this band will @ 835 cm⁻¹ for BN2 and 848 cm⁻¹ for BN, having Raman intensities that are not excessive. In spite of the DFT, The estimated recurrence interval matches the measured value of Because of this, I was surprised to find out how common this mode is in BN2. with the use of DFTs.

TABLE 3: Calculated and Observed Frequencies (ν , in cm^{-1}), Raman Intensities (I), and Depolarization Ratios (ρ) of BN

symmetry	calcd			obsd			assignment ^d
	ν^a	I^b	ρ^a	ν^b	ν^c	ρ^c	
B	1630	1.3	0.75	1619			$\nu_{C_1-C_2}, \nu_{C_2-O_{11}}, \nu_{C_3-C_4}, \nu_{C_5-C_6}, \nu_{C_7-C_8}, \delta O-H$
A	1606	211	0.48	1591	1588	0.47	$\nu_{C_1-C_1}, \nu_{C_2-C_3}, \nu_{C_6-C_7}, \nu_{C_9-C_{10}}, \delta O-H$
A	1498	38	0.05	1517			$\nu_{C_2-O_{11}}, \delta C_3-H, \delta C_7-H$
A	1454	48	0.37	1470	1470	~0.20	$\nu_{C_7-C_8}, \nu_{C_1-C_9}, \nu_{C_{10}-C_5}$
B	1451	34	0.75	1440			$\nu_{C_7-C_8}, \nu_{C_1-C_9}, \nu_{C_{10}-C_5}$
A	1387	199	0.03	1378	1377	0.15	$\nu_{C_9-C_{10}}, \delta O-H, \nu_{C_2-O_{11}}$
A	1305	40	0.01	1308			$\nu_{C_1-C_1}, \delta O_{11}-H$
A	1287	5.5	0.745	1274	1282	~0.40	$\nu_{C-O}, \nu_{C_8-C_9}, \delta C_5-H, \delta C_7-H, \delta C_8-H$
B	1254	2.3	0.75	1255			$\delta C_5-H, \delta C_8-H$
B	1214	5.6	0.75	1213			$\delta O_{11}-H$
A	1158	12	0.69	1147	1145	~0.50	$\delta C_6-H, \delta C_5-H, \delta C_4-H, \delta C_7-H$
A	1076	7.4	0.02	1067	1067		$\nu_{C_1-C_1}, \delta C_7-C_8-C_9, \delta C_{10}-C_5-C_6, \delta C_4-H$
A	1037	24	0.04	1025	1027	0.17	$\nu_{C_6-C_7}, \delta C_6-C_7-C_8, \delta C_5-C_6-C_7, \delta C_5-H, \delta C_6-H, \delta C_7-H, \delta C_8-H$
A	957	9.1	0.18	952	964	0.11	$\delta C_1-C_2-C_3, \delta C_{10}-C_5-C_6, \delta C_6-C_7-C_8, \delta C_8-C_9-C_{10}$
A	848	23	0.05	847	849	0.05	$\delta C_3-C_4-C_{10}, \delta C_6-C_7-C_8$
B	790	12	0.75	794			$\gamma_{C_8-H}, \gamma_{C_3-H}, \gamma_{C_4-H}, \gamma_{C_5-H}$
A	668	27	0.07	664	666	0.06	$\delta C_7-C_8-C_9, \delta C_{10}-C_5-C_6$
A	581	5.2	0.13	582	584	0.10	$\tau_{C_1}, \tau_{C_2}, \tau_{C_4}, \tau_{C_{10}}, \tau_{C_3}, \gamma_{C_3-H}, \gamma_{C_4-H}, \gamma_{C_6-H}, \gamma_{C_8-H}, \gamma_{C_5-H}$
A	533	12	0.12	531	531		$\delta C_6-C_7-C_8, \delta C_9-C_{10}-C_5, \delta C_2-C_3-C_4$
B	523	9.4	0.75	522			$\delta C_6-C_7-C_8, \delta C_9-C_{10}-C_5, \delta C_2-C_3-C_4$
A	508	5.4	0.16	509			$\tau_{C_9}, \tau_{C_{10}}, \tau_{C_1}, \tau_{C_4}, \gamma_{C_4-H}, \gamma_{C_5-H}, \gamma_{C_8-H}, \delta O_{11}H$
B	485	3.5	0.75	490			$\tau_{C_9}, \tau_{C_{10}}, \tau_{C_5}, \tau_{C_8}, \gamma_{C_5-H}, \gamma_{C_8-H}, \gamma_{C_4-H}$
B	523	9.4	0.75	522			$\delta C_6-C_7-C_8, \delta C_9-C_{10}-C_5, \delta C_2-C_3-C_4$
A	508	5.4	0.16	509			$\tau_{C_9}, \tau_{C_{10}}, \tau_{C_1}, \tau_{C_4}, \gamma_{C_4-H}, \gamma_{C_5-H}, \gamma_{C_8-H}, \delta O_{11}H$
B	485	3.5	0.75	490			$\tau_{C_9}, \tau_{C_{10}}, \tau_{C_5}, \tau_{C_8}, \gamma_{C_5-H}, \gamma_{C_8-H}, \gamma_{C_4-H}$
A	434	10	0.10	437	435	0.32	$\tau_{C_9}, \tau_{C_{10}}, \tau_{C_5}, \tau_{C_8}, \gamma_{C_5-H}, \gamma_{C_8-H}$
A	423	5.0	0.57	416			$\tau_{C_9}, \tau_{C_{10}}, \tau_{C_5}, \tau_{C_8}, \gamma_{C_5-H}, \gamma_{C_8-H}$
A	364	3.4	0.71	374			$\tau_{C_5}, \tau_{C_8}, \tau_{C_3}, \gamma_{C_5-H}, \gamma_{C_8-H}, \gamma_{C_3-H}$
A	346	4.3	0.64	349			$\tau_{C_4}, \tau_{C_1}, \tau_{C_2}, \tau_{C_3}, \tau_{C_9}, \gamma_{C_4-H}, \gamma_{C_7-H}, \gamma_{O_{11}H}$
A	232	1.5	0.66	245			$\gamma O-H$ τ_{butt}

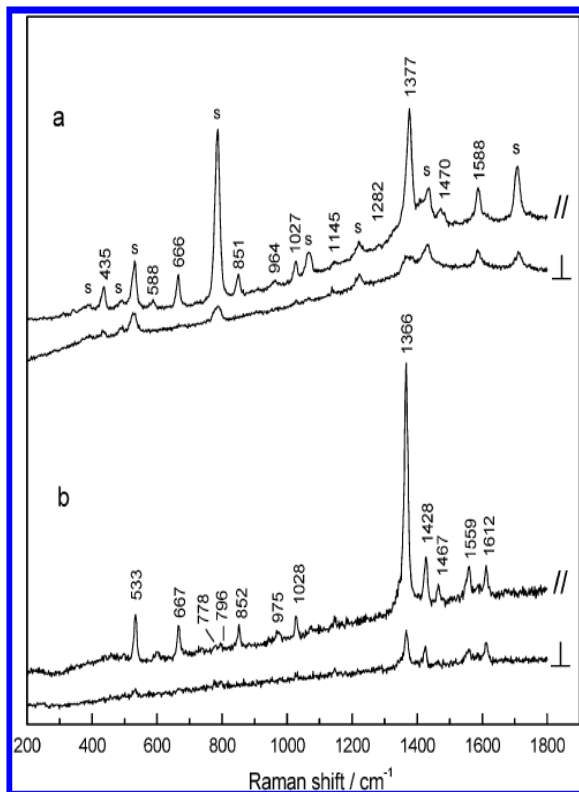
a Calculated with B3LYP/6-31G*; frequency scaling factor) 0.98. *b* From solid Raman spectra excited at 514.5 nm. *c* From solution Ramanspectra (in acetone) excited at 514.5 nm. *d* Mode assignments: \hat{i} , bond stretching; \hat{a} , in-plane (naphthyl) bond bending; ζ , out-of-plane (naphthyl) wagging of hydrogen atoms; \hat{o} , out-of-plane (naphthyl) torsion of carbon atoms; $\hat{o}butt$, butterfly torsion between two naphthyl rings.

TABLE 4: Calculated and Observed Frequencies (ν , in cm^{-1}), Raman Intensities (I), and Depolarization Ratios (ρ) of BN²⁻

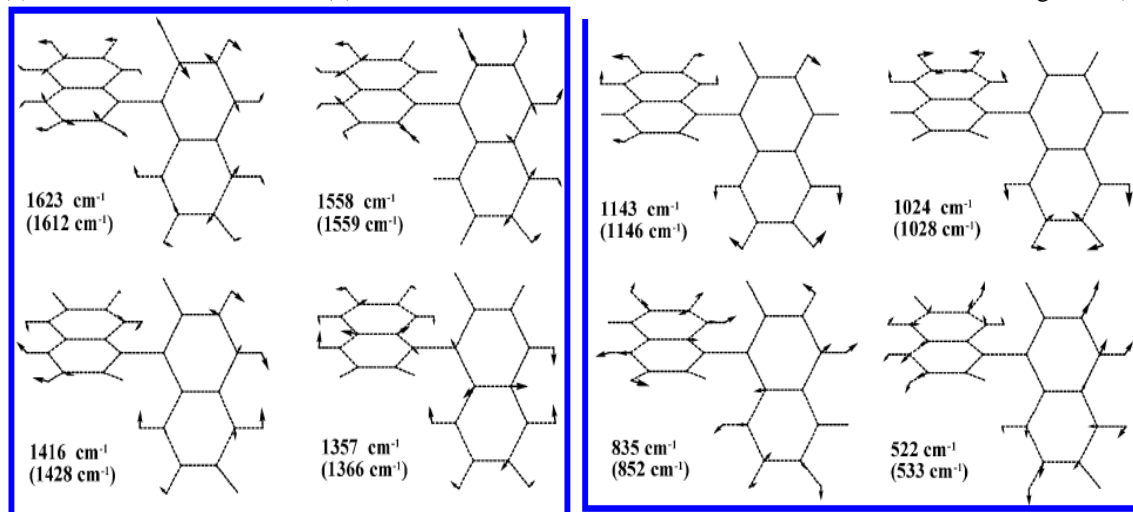
symmetry	calcd			obsd			assignment ^d
	ν^a	I^b	ρ^a	ν^b	ν^c	ρ^b	
A	1623	57	0.14	1612	1612	0.57	$\nu_{C_2-O_{11}}, \nu_{C_3-C_4}, \nu_{C_5-C_6}, \nu_{C_7-C_8}$
A	1611	181	0.70	1592	1590	0.55	$\nu_{C_7-C_8}, \nu_{C_3-C_4}, \nu_{C_{10}-C_5}$
A	1558	90	0.34	1559	1557	0.37	$\nu_{C_2-O_{11}}, \nu_{C_3-C_4}, \nu_{C_3-C_4}$
A	1525	27	0.43	1549		0.52	$\nu_{C_7-C_8}, \nu_{C_3-C_4}, \nu_{C_3-C_4}, \delta C_7-H$
A	1500	163	0.18	1502			$\nu_{C_3-C_4}, \nu_{C_{10}-C_5}, \delta C_7-H, \delta C_3-H$
A	1453	102	0.63	1467	1466	0.34	$\nu_{C_1-C_9}, \nu_{C_3-C_4}, \delta C_7-H, \delta C_3-H, \delta C_1-H$
B	1444	9.0	0.75	1455			$\nu_{C_1-C_9}, \nu_{C_3-C_4}, \delta C_7-H, \delta C_3-H, \delta C_1-H$
A	1416	117	0.71	1428	1428	0.40	$\nu_{C_2-C_3}, \nu_{C_3-C_4}, \nu_{C_7-C_8}, \delta C_3-H, \delta C_1-H$
A	1357	135	0.14	1366	1366	0.15	$\nu_{C_7-C_8}, \nu_{C_3-C_4}, \nu_{C_3-C_4}$
A	1297	96	0.08	1287			$\nu_{C_1-C_1}, \nu_{C_1-C_1}$
A	1234	69	0.23	1244			$\nu_{C_1-C_3}, \nu_{C_{10}-C_5}, \delta C_3-H, \delta C_3-H$
A	1218	26	0.47	1215			$\nu_{C_{10}-C_5}, \nu_{C_3-C_4}, \delta C_7-H, \delta C_3-H$
A	1156	12	0.48	1187			$\nu_{C_1-C_1}, \delta C_7-H, \delta C_7-H$
A	1143	30	0.69	1146	1150	~0.50	$\delta C_7-H, \delta C_7-H$
A	1128	11	0.27	1132			$\delta C_7-H, \delta C_7-H, \delta C_7-H$
A	1049	51	0.16	1073	1074	~0.25	$\nu_{C_1-C_1}, \delta C_7-H, \delta C_7-H, \delta C_7-H$
A	1024	48	0.26	1028	1029	0.18	$\nu_{C_7-C_8}, \delta C_7-C_8, \delta C_3-C_4-C_5, \delta C_3-H, \delta C_3-H, \delta C_7-H$
A	975	5.4	0.09	975	980	0.30	$\delta C_1-C_9-C_{10}, \delta C_6-C_7-C_8, \delta C_1-C_1-C_1$
B	949	0.8	0.75	935			$\delta C_1-C_1-C_3, \delta C_1-H$
A	835	25	0.05	852	850	0.06	$\delta C_1-C_1-C_{10}, \delta C_6-C_7-C_8, \delta C_3-C_4-C_7$
B	805	2.6	0.75	796			$\gamma_{C_7-H}, \gamma_{C_1-H}, \gamma_{C_3-H}, \gamma_{C_4-H}, \tau_{C_4}, \tau_{C_3}$
B	760	14	0.75	778			$\nu_{C_9-C_{10}}, \gamma_{C_7-H}, \gamma_{C_4-H}, \gamma_{C_3-H}, \gamma_{C_4-H}$
A	730	9.2	0.73	737	739	~0.67	$\delta C_1-C_1-C_3, \delta C_3-C_4-C_7$
A	659	41	0.18	667	666	0.19	$\tau_{C_3}, \tau_{C_6}, \gamma_{C_7-H}, \gamma_{C_4-H}, \gamma_{C_3-H}$
A	522	32	0.10	533	534	0.16	$\delta C_6-C_7-C_8, \delta C_9-C_{10}-C_5, \delta C_2-C_3-C_4$

a Calculated with B3LYP/6-31G*; frequency scaling factor) 0.98. *b* From solution Raman spectrum (in 3 M NaOH) excited at 514.5 nm. *c* From solution Raman spectra (in 3 M NaOH) excited at 325 nm. *d* Mode assignments: \hat{i} , bond

stretching; \tilde{a}_i , in-plane (naphthyl) bond bending; ζ , out-of-plane (naphthyl) wagging of hydrogen atoms; \tilde{o} , out-of-plane (naphthyl) torsion of carbon atoms. The two weak Raman bands at 796 and 778 cm^{-1} of BN2- have the depolarization ratios approximately 0.75 and are consequently considered as belonging to the asymmetry vibrations. On the basis of the agreement of estimated and observed frequencies and depolarization ratios, we provisionally allocate these two bands to the computed vibrations of BN2- at 805 and 760 cm^{-1} . According to the DFT calculations, the vibration estimated at 760 cm^{-1} is due to the in-plane breathing mode of naphthyl ring (Scherer's $\tilde{8}$ mode for naphthalene), while the one at 805 cm^{-1} is attributable to the C-H out-of-plane wiggling mode



of naphthyl ring. **Figure 4.** Polarized Raman spectra of BN (a) in an acetone solution; (b) in a 3 M NaOH solution with the excitation wavelength (λ_{ex}) 514.5 nm.



Figure

5. Schematic diagram showing the Cartesian displacements of selected Raman active modes of BN²⁻ calculated with B3LYP/6-31G*.

The calculated (plain text) and the measured (in parenthesis) frequencies have been shown for each mode. A strong Raman band with A symmetry is predicted by DFT calculations for BN₂ at 659 cm⁻¹. This mode is assigned to the 667 cm⁻¹ strong band of BN₂. The Cartesian atomic number This mode's displacements point to the C-H out-of-plane wagging. This experiment's depolarization ratio was found to be 19. According to the estimated value, modes are in agreement (0.18). Its opposite Consistent with this finding, BN was seen at 666 cm⁻¹. by doing a DFT calculation There was a prominent Raman band in the low-frequency area of the spectrum. BN²⁻ (in a 3 M NaOH solution) was detected at 533 cm⁻¹ and with respect to the BN solid, at 531 cm⁻¹. The BN Raman spectrum Raman spectroscopy, this band is overlapped by an acetone solution. of acetone We attribute it to the naphthyl deformation that occurs in-plane. Scheler's naphthalene $\hat{i}33$ mode, which came up with a value of 522 cm⁻¹ for BN²⁻, and 533 cm⁻¹ for BN. ' Experimentation's worth This mode's depolarization ratio in BN₂ is 0.16, which is compatible within accordance with the estimated value (0.10). In the solid state, there existed a 435 cm⁻¹ Raman band for BN. both in their natural condition and in an acetone solution. In the blink of an eye, this band had entirely disbanded in the neighbourhood of BN₂. We believe it to be an O-H out-of-plane anomaly. a swaying motion. DFT calculations indicate a very skewed result. O-H rocking vibrations at a lower, more manageable frequency At a distance of 346 cm⁻¹, Calculation versus experimentation is the difference. believes that this is because hydrogen bonding has been overlooked. that is predicted to occur in the calculating model in order to have a major impact on O-H rocking out of plane. modes of BN molecule DFT computing has been used in the preceding investigations to provide semiquantitative results. forecasts of the change in vibrational frequency Deprotonation of hydroxyls in BN causes bands. The The effects of deprotonation on intensity and depolarization are also readily apparent. Figures show the ratios and other features of Raman bands There are three and four of them). This is something that has not been addressed in this work, and it should be. because of the deprotonation phenomenon, should be examined further are crucial to the success of a project.

UV Near-Resonance Raman Spectra (UVRRS) Excited at 325 nm.

The 900-1620 cm⁻¹ area of the 325 nm excited resonance Raman spectra of BN in basic solution revealed numerous peculiarities (Figure 3a). Figure 3a illustrates this. the BN Raman band at 1612 cm⁻¹ in basic solution amazing improvement, much more powerful than the 1366 band cm⁻¹. This significant increase in resonance might be the consequence of Raman scattering and the approximate double resonance Tsuboi's law of near-resonance enhancing mentioned in the following paragraphs. For starters, the double resonance is defined 32. shows an increase in the scattered photon's intensity where I the energy of the photons, ρ_1 both the incident and scattering photons' ρ_2 are in agreement. as well as (ii) the two excitation energy levels Vibrational frequency differences are equivalent to the difference between $p(\delta_1 - \delta_2)$ of a single molecule. Using third-order time dependent models, Peticolas et al. 33,

The Raman transition may be calculated using perturbation theory.

$$\alpha_{gf,gi}^{\rho\sigma} = - \sum_{e,s} \left\{ \frac{M_{ge}^{\rho} h_{es} M_{sg}^{\sigma} \langle f|Q|i \rangle}{[E_e^0 - E_g^0 + (f-i)\hbar\Omega - \hbar\omega_L][E_s^0 - E_g^0 - \hbar\omega_L]} + \text{c.c.} \right\} \quad (1)$$

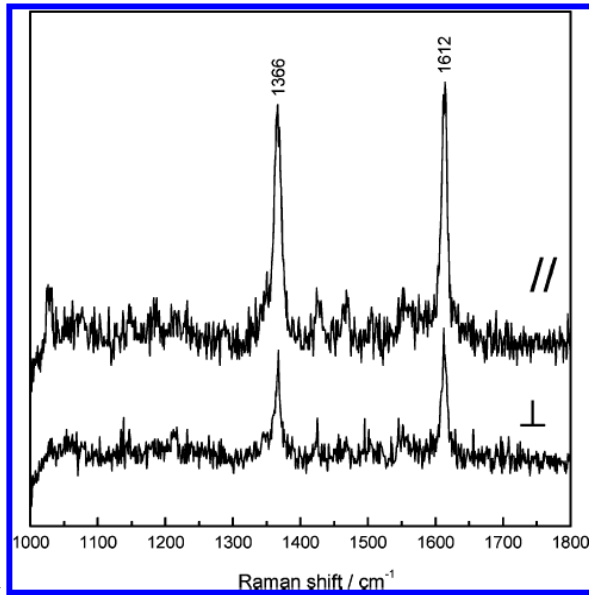
where M_{ge}^{ρ} , h_{es} , and M_{sg}^{σ} are the electronic ground and excited states at Q respectively, Q is the normal vibration coordinate, and j and i are initial and final vibration states in the ground electronic state. Because the sum over vibrational levels does not appear in eq 1, this expression also contains

$$A_{gf,gi}^{\rho\sigma} = - \sum_e \left\{ \frac{M_{ge}^{\rho} h_{ee} M_{eg}^{\sigma} \langle f|Q|\hat{i} \rangle}{[E_e^0 - E_g^0 - (\hbar\omega_L - (f-i)\hbar\Omega)][E_e^0 - E_g^0 - \hbar\omega_L]} + c.c. \right\} \quad (2)$$

a “trace” (e) s) B type term

completely symmetric modes. From UV absorption spectra of BN in a 3 M NaOH aqueous solution (Figure 2), the incoming photon energy (325 nm) is virtually resonant to the longest-wavelength absorption peak about 358 nm, and the scattered photon energy (1612 cm⁻¹) for the 1612 cm⁻¹ mode is more close to the absorption peak, so, on the basis of eq 2, $A_{gf,gi}^{\rho\sigma}$ is approximated double-resonance enhancement. Also, eq 2 suggests that the 1612 cm⁻¹ band is more favourably improved than that at 1366 cm⁻¹, because the scattering photon energy for the 1612 cm⁻¹ band is near the absorption peak. We can use eq 1 to make comparable and qualitative talks on other B terms, since two excitation energy levels E_e^0 and E_s^0 of BN in an acetone solution come from the excitonic splitting of two degenerate levels and $(\delta_1 - \delta_2) |E_s^0 - E_e^0| = 0.22$ eV (1775 cm⁻¹),^{14,19} which is nearly comparable to the frequency of the 1612 cm⁻¹ band and meets the above condition (ii) (ii). Here, we have assumed that for BN in basic solution $|E_s^0 - E_e^0| = 0.22$ eV. The foregoing doubly resonant feature is worth examining further, since strong resonance improvement, better assignment of modes by their selected resonance enhancement, and potential deduction of vibronic connections for the modes are known to be the benefits of doubly resonant Raman spectroscopy.^{14,32} Second, on the basis of actual findings of various molecules, Hirakawa and Tsuboi³⁵ developed the termed Tsuboi’s rule: “If a Raman line grows stronger as the excitation line is moved closer to the frequency of an electronic band Ar X, then the equilibrium conformation of the molecule is warped along the normal coordinate for the Raman line in the transition from the ground state (X) to the excited state (A).” On the basis of a similar approach, Markham et al. made an initial calculation of the dimensionless displacement parameters. It described convincingly the impact of deuterium substitution on RR spectra of imidazole and imidazolium.²²

The related electromagnetic spectrum of BN arises from the conjugated $\pi \rightarrow \pi^*$ transition of naphthol chromophore.^{18,19} According to the foregoing theoretical explorations of the conjugate anionic bases of hydroxyaryls, the S0 \rightarrow S1 excitation of naphtholate and phenolate induces large immigration of electron from the oxygen atom to the distal rings. This is predicted to result in large alterations for the distances of the C2-O11 bond. Our DFT computation indicates that the 1612 cm⁻¹ mode involves a strong contribution from the stretching of C2-O11 bonds, so according to Tsuboi rule, the 1612 cm⁻¹ band is favourably resonant increased at the excitation (325 nm). For further work, quantitative calculations of RR intensity are needed to account for the resonance enhancement without immediately resorting to the idea of double resonance enhancement. Resonance Raman intensities have been well-formulated either in a traditional sum-over-state picture^{39,34} or equivalently in the time-dependent resonance Raman formulas.^{40,41} Although they are theoretically equivalent with each other, the



time dependent **Figure 6.** Polarized Raman spectrum of BN in a 3 M NaOH aqueous solution with the excitation wavelength λ_{ex} 325 nm.

For systems with a large number of vibrational modes, the time-dependent technique has been shown to be more efficient in computing. For one enthusiastic person is involved in the near-resonance scenario discussed in this study, they've contributed to the RR intensity by being in an intermediate state not yet properly recognised. Thus, making a decision is challenging, employing a time-dependent approach for direct quantitative computing of the RR scattering.^{40, 42} Departures from the normal bands such as 1612 cm⁻¹ have a distinct intensity pattern BN₂-band following RR spectra modelling utilising time-dependent. Additional resonance enhancement using the RR technique. The mechanisms may need thorough examination. The energy denominator in RR formulas⁴² features such as this one. This part is finished. Polarization is a key component of this section. UVRR Spectra's properties. The loss of polarity in resonance, the ratio of the 1366 and 1612 cm⁻¹ bands BN₂-Raman spectra at 325 nm (ex) were found to be 0.42, 0.15 and 0.57, respectively, in conventional Raman spectroscopy. At 514.5 nm, as shown in Figure 4b, respectively, we can discern spectra. The polarisation qualities are described by the depolarization F , expresses itself

$$\rho = \frac{5\sum^1 + 3\sum^2}{10\sum^0 + 4\sum^2} = \frac{5(\sum^1/\sum^2) + 3}{10(\sum^0/\sum^2) + 4} \quad (3)$$

in the form of²⁰

where Placzek invariants \square_0 , \square_2 , and \square_4 describe the isotropic, symmetric anisotropy, and antisymmetric part of the Raman tensors, respectively

$$\begin{aligned} \sum^0 &= \frac{1}{3} |\alpha_{xx} + \alpha_{yy} + \alpha_{zz}|^2 \\ \sum^1 &= \frac{1}{2} \{ |\alpha_{xy} - \alpha_{yx}|^2 + |\alpha_{xz} - \alpha_{zx}|^2 + |\alpha_{yz} - \alpha_{zy}|^2 \} \\ \sum^2 &= \frac{1}{2} \{ |\alpha_{xy} + \alpha_{yx}|^2 + |\alpha_{xz} + \alpha_{zx}|^2 + |\alpha_{yz} + \alpha_{zy}|^2 \} + \\ &\quad \frac{1}{3} \{ |\alpha_{xx} - \alpha_{yy}|^2 + |\alpha_{xx} - \alpha_{zz}|^2 + |\alpha_{yy} - \alpha_{zz}|^2 \} \quad (4) \end{aligned}$$

It is known that in normal Raman spectra, antisymmetric transition polarizability or ρ_1 is zero, but in resonance Raman scattering, ρ_1 can be nonzero. Thus, for the normal Raman spectra, the depolarization ratio ρ' is and in resonance cases.

$$\rho' = \frac{3}{4 + 10(\sum^0/\sum^2)} \quad (5) \quad \rho = \rho' + \frac{5(\sum^1/\sum^2)}{4 + 10(\sum^0/\sum^2)} \quad (3')$$

$F = 0.42$
> $F = 0.15$ for the 1366 cm⁻¹ band of BN₂- and $F = 0.47$ – $F = 0.57$ for the 1612 cm⁻¹ band. Therefore, for the 1366 cm⁻¹ band of BN₂-, not only the symmetric part contributes to this band but also the antisymmetric part; however, the 1612 cm⁻¹ band does not include an antisymmetric Raman scattering contribution. The result for the 1366 cm⁻¹ band of BN₂- agree with DR-SFV spectra of BN₂, in which the 1377 cm⁻¹ band of BN (corresponding to 1366 cm⁻¹ of BN₂-) is most intensive and the strength of DR-SFVS from isotropic chiral liquids is proportional to the square of the corresponding antisymmetric Raman scattering tensor. But the 1612 cm⁻¹ band is beyond the measured frequency region of DR-SFVS in ref 14 and needs to be further investigated by the DR-SFVS method. For the 1366 cm⁻¹ band of BN₂- in the normal Raman spectra, $F = 0.15$, and so by use of eq 5

$$\sum^0/\sum^2 = 1.6 \quad (6)$$

Since in resonance cases $F = 0.42$, using eqs 3, 6 and 5,

$$\sum^1/\sum^2 = 1.08 \quad (7)$$

we get. From eqs 4 and 7, we can estimate the order of magnitude for the ratio K between antisymmetric (R_{anti}) and symmetric transition polarizabilities (R_{sym})

$$K = \frac{\alpha_{anti}}{\alpha_{sym}} \approx (\sum^1/\sum^2)^{(1/2)} = 1.04 \quad (8)$$

On the basis of the nonadiabatic correction terms of antisymmetric transition polarizability, Buckingham and Liu^{36,37} gave the following formula of the order of

$$K' = \frac{\alpha_{anti}}{\alpha_{sym}} \approx \frac{\hbar\Omega}{E_e^0 - E_s^0} \quad (9)$$

magnitude of R_{anti}/R_{sym} where E_e^0 and E_s^0 are the energies of the excitation electronic states coupled by the mode p_i , and Ω is the frequency of the vibration band. Here, for the

1366 cm⁻¹ band, from the absorption spectra of BN in acetone solution,^{19,14} the two peaks in the absorption spectrum come from transitions to the two exciton states separated by 0.22 eV, which corresponds to ($E_{e0} - E_s$) in

$$K' \approx \frac{1366}{0.22 \times 8065.7} = 0.77 \quad (10)$$

the above equation,¹⁴ thus

Eqs. 8 and 10 reveal that the near-degeneracy of the excited-state levels (excitonic splittings) is critical for the experiment and theory to accord qualitatively. BN's transition polarizability is antisymmetric. The nonresonance Raman scattering of tetrahydrofuran occurs in the large-amplitude vibration modes of the $\hat{1}6$ groups. BN²⁻ has 38 more bands, including 935, 1074, 1150, 1187, and 1187. Resonance is also seen at 1215 cm⁻¹, 1244 cm⁻¹, and 1287 cm⁻¹. but cannot be quantified with certainty in the near-resonance water solution with 3M NaOH and polarised Raman spectra of bismuth (BN). Figure 6 shows the answer. Antisymmetric Raman scattering is currently being investigated in this topic. Qualitative and preliminaries. To discuss the antisymmetrical role of polarizability in an SFG with two double-resonant modes we need to do further research before conducting a direct Raman spectroscopic analysis, both in terms of actual measures and theoretically derived ones. In broad experimental considerations in general, when isotropic, symmetric, and homogeneous a given Raman band is formed through antisymmetric scattering. Circular measurement of the reversal coefficient is required. Dispersion of polarised light at an angle of 180 degrees to directly and ii) RR excitation, quantitatively distinguish 0, 2, and 1.20 to plot profiles and dispersion curves for a certain Raman band. Historically, bands have played a significant role in both theoretical and experimental investigation. Crucial work done by the RR spectrum group²⁰ due to the lack of resonance in antisymmetric Raman scattering. The slope of the antisymmetric Raman tensors is substantially steeper than that of the ones that are symmetrical due to the time-reversal symmetry arguments³⁷ or the effects of interference from various vibronic transitions.²⁰ Quantitative analysis may be found in RR spectra theory. Calculations of RR intensity, depolarization ratios, and their order to take into consideration the frequency dependency of the excitation frequencies for a better sound quality. Then, there's the addition of BN. Dr-SFVS and RRR spectrums should be used to look at systems in depth.

Conclusions

For the first time, we have analysed the normal and UV near-resonance Raman (UVRR) spectra of 1,1-bi-2-naphthol (BN). Raman scattering of acetone-based BN in the presence of polarised BN. We also looked at the effects of BN and B in a 3 M NaOH aqueous solution. Calculations were made using density functional theory to investigate the vibrational frequencies and the condition of the matter structure of BN²⁻. The Raman band assignments noticed are based on measurements and calculations, and as a result, intensities and depolarization ratios. Analyzed by us 1612 and 1612 BN basic solution depolarization ratios. Normal and UV resonance Raman spectra show 1366 cm⁻¹ and 1612 cm⁻¹ bands, suggesting that symmetry and antisymmetry were both possible. The 1366 cm⁻¹ band is mostly made up of Raman tensor contributions, however the 1612 cm⁻¹ band is made up entirely of the symmetrical portion of this signal.

Acknowledgment.

We are grateful to Professor A. D. Buckingham for very helpful comments on this paper. This work was supported by the National Natural Science Foundation of China (Grant 20473078, 20173051) and the Development Foundation of the Education Department of China (Grant 20020358061).

References

- (1) Chen, Y.; Yekta, S.; Yudin, A. K. *Chem. Rev.* **2003**, *103*, 3155.

- (2) Pu, L. *Chem. ReV.* **1998**, 98, 2405.
- (3) Shibasaki, M.; Sasai, H.; Arai, T. *Angew. Chem., Int. Ed.* **1997**, 36, 1236.
- (4) (a) Eilerts, N. W.; Heppert, J. A. *Polyhedron* **1995**, 14, 3255. (b) Rosini, C.; Franzini, L.; Raffaelli, A.; Salvadori, P. *Synthesis* **1992**, 503.
- (5) (a) Ishii, A.; Soloshonok, V. A.; Mikami, K. *J. Org. Chem.* **2000**, 65, 1597. (b) Griffith, W. P.; Nogueira, H. I. S.; White, A. J. P.; Williams, D. J. *Polyhedron* **1997**, 16, 1323. (c) Whitesell, J. K. *Chem. ReV.* **1989**, 89, 1581. (d) Bringmann, G.; Walter, R.; Weirich, R. *Angew. Chem., Int. Ed.* **1990**, 29, 977.
- (6) (a) Kyba, E. P.; Gokel, G. W.; Jong, F. de; Koga, K.; Sousa, L. R.; Siegel, M. G.; Kaplan, L.; Sogah, G. D. Y.; Cram, D. J. *J. Org. Chem.* **1977**, 42, 4173. (b) Yudin, A. K.; Martyn, L. J. P.; Pandiaraju, S.; Zheng, J.; Lough, A. *Org. Lett.* **2000**, 2, 41.
- (7) Setnic'ka, V.; Urbanova', M.; Bour', P.; Kra'l, V.; Volka, K. *J. Phys. Chem. A* **2001**, 105, 8931.
- (8) Sahnoun, R.; Koseki, S.; Fujimura, Y. *J. Mol. Struct.* **2005**, 735-736, 315.
- (9) Nogueira, H. I. S.; Quintal, S. M. O. *Spectrochim. Acta, Part A* **2000**, 56, 959.
- (10) Fischer, P.; Wiersma, D. S.; Righini, R.; Champagne, B.; Buckingham, A. D. *Phys. ReV. Lett.* **2000**, 85, 4253.
- (11) Belkin, M. A.; Kulakov, T. A.; Ernst, K.-H.; Yan, L.; Shen, Y. R. *Phys. ReV. Lett.* **2000**, 85, 4474.
- (12) (a) Belkin, M. A.; Han, S. H.; Wei, X.; Shen, Y. R. *Phys. ReV. Lett.* **2001**, 87, 113001. (b) Ji, N.; Ostroverkhov, V.; Belkin, M. A.; Shiu, Y. J.; Shen, Y. R. *J. Am. Chem. Soc.* **2006**, 128, 8845.
- (13) Fischer, P.; Buckingham, A. D.; Albrecht, A. C. *Phys. ReV. A* **2001**, 64, 053816.
- (14) Belkin, M. A.; Shen, Y. R. *Phys. ReV. Lett.* **2003**, 91, 213907. (15) Fischer, P.; Wise, F. W.; Albrecht, A. C. *J. Phys. Chem. A* **2003**, 107, 8232.
- (16) (a) Buckingham, A. D.; Fischer, P. *Chem. Phys. Lett.* **1998**, 297, 239. (b) Fischer, P.; Buckingham, A. D.; Beckwith, K.; Wiersma, D. S.; Wise, F. W. *Phys. ReV. Lett.* **2003**, 91, 173901.
- (17) (a) Belkin, M. A.; Shen, Y. R. *Int. ReV. Phys. Chem.* **2005**, 24, 257. (b) Fischer, P.; Hache, F. *Chirality* **2005**, 17, 421.
- (18) Zheng, R.-H.; Chen, D.-M.; Wei, W.-M.; He, T.-J.; Liu, F.-C. *J. Phys. Chem. B.* **2006**, 110, 4480.
- (19) Byers, J. D.; Hicks, J. M. *Chem. Phys. Lett.* **1994**, 231, 216.
- (20) Mortensen, O. S.; Hassing, S. *Adv. IR Raman Spectrosc.* **1980**, 6, 1.
- (21) (a) Becke, A. D. *J. Chem. Phys.* **1993**, 98, 5648. (b) Lee, C.; Yang, W.; Parr, R. G. *Phys. ReV. B* **1988**, 37, 785.
- (22) Markham, L. M.; Mayne, L. C.; Hidson, B. S.; Zgierski, M. Z. *J. Phys. Chem.* **1993**, 97, 10319.
- (23) (a) Scott, A. P.; Radom, L. *J. Phys. Chem.* **1996**, 100, 16502. (b) Oakes, R. E.; Spence, S. J.; Bell, S. E. J. *J. Phys. Chem. A* **2003**, 107, 2964. (c) Xu, L.-C.; Li, Z.-Y.; Tan, W.; He, T.-J.; Liu, F.-C.; Chen, D.-M. *Spectrochim. Acta, Part A* **2005**, 62, 850.

- (24) Pasterny, K.; Wrzalik, R.; Kupka, T.; Pasterna, G. *J. Mol. Struct.* **2002**, 614, 297
- (25) Devlin, F. J.; Stephens, P. J.; O[−]sterle, C.; Wiberg, K. B.; Cheeseman, J. R.; Frisch, M. J. *J. Org. Chem.* **2002**, 67, 8090.
- (26) Frisch, M. J.; Trucks, G. W.; Schlegel, H. B.; Scuseria, G. E.; Robb, M. A.; Cheeseman, J. R.; Montgomery, J. A., Jr.; Vreven, T.; Kudin, K.N.; Burant, J. C.; Millam, J. M.; Iyengar, S. S.; Tomasi, J.; Barnone, V.; Mennucci, B.; Cossi, M.; Scalmani, G.; Nega, N.; Petersson, G. A.; Nakatsuji, H.; Haha, M.; Ehara, M.; Toyota, K.; Fukuda, R.; Hasegawa, J.; Ishida, M.; Nakajima, T.; Honda, Y.; Kitao, O.; Nakai, H.; Klene, M.; Li, X.; Knox, J. E.; Hratchian, H. P.; Cross, J. B.; Adamo, C.; Jaramillo, J.; Gomperts, R.; Stratmann, R. E.; Yazyev, O.; Austin, J.; Cammi, R.; Pomelli, C.; Ochterski, J. W.; Ayala, P. Y.; Morokuma, K.; Voth, G. A.; Salvador, P.; Dannenberg, J. J.; Zakrzewski, V. G.; Dapprich, S.; Daniels, A. D.; Strain, M. C.; Farkas, O.; Malick, D. K.; Rabuck, A. D.; Raghavachari, K.; Foresman, J. B.; Ortiz, J. V.; Cui, Q.; Baboul, A. G.; Clifford, S.; Cioslowski, J.; Stefanov, B. B.; Liu, G.; Liashenko, A.; Piskorz, P.; Peng, C. Y.; Nanayakkara, A.; Challacombe, M.; Gill, P. M. W.; Johnson, B.; Chen, W.; Wong, M. W.; Gonzales, C.; Pople, J. A. *Gaussian 03*, revision B.03; Gaussian, Inc.: Pittsburgh, PA, 2003.
- (27) Mori, K.; Masuda, Y.; Kashino, S. *Acta Crystallogr., Sect. C* **1993**, 49, 1224.
- (28) Agmon, N.; Rettig, W.; Groth, C. *J. Am. Chem. Soc.* **2002**, 124, 1089.
- (29) Granucci, G.; Hynes, J. T.; Millie', P.; Tran-Thi, T.-H. *J. Am. Chem. Soc.* **2000**, 122, 12243
- (30) Scherer, J. R. *J. Chem. Phys.* **1962**, 36, 3308.
- (31) Didi, M. A.; Maki, A. K. T.; Mostafa, M. M. *Spectrochim. Acta, Part A* **1991**, 47, 667.
- (32) Ivchenko, E. L. *Optical Spectroscopy of Semiconductor Nanostructure*; Alpha Science: Harrow, UK, 2005; section 6.7.
- (33) Peticolas, W. L.; Nafie, L.; Stein, P.; Fanconi, B. *J. Chem. Phys.* **1970**, 52, 1576.
- (34) Johnson, B. B.; Peticolas, W. L. *Annu. Rev. Phys. Chem.* **1976**, 27, 465, eq. 25.
- (35) Hirakawa, A. Y.; Tsuboi, M. *Science* **1975**, 188, 359.
- (36) Liu, F.-C. *J. Phys. Chem.* **1991**, 95, 7180.
- (37) Liu, F.-C.; Buckingham, A. D. *Chem. Phys. Lett.* **1993**, 207, 325.
- (38) Li, L.; He, T.-J.; Wang, X.-Y.; Zuo, J.; Xu, C.-Y.; Liu, F.-C. *Chem. Phys. Lett.* **1996**, 262, 52
- (39) Tang, J.; Albrecht, A. C. In *Raman Spectroscopy*; Szymanski, H.A., Ed.; Plenum: New York, 1970; Vol. 2, Chapter 2.
- (40) Lee, S.-Y.; Heller, E. J. *J. Chem. Phys.* **1979**, 71, 4777. (41) (a) Myers, A. B. *J. Raman Spectrosc.* **1997**, 28, 389. (b) Leng, W.; Wurthner, F.; Kelley, A. M. *J. Phys. Chem. B* **2004**, 108, 10284.
- (42) Chen, D.-M.; He, T.-J.; Cong, D.-F.; Zhang, Y.-H.; Liu, F.-C. *J. Phys. Chem. A* **2001**, 105, 3981.